Switching Field Distribution of MnGa Bit Patterned Film Fabricated by Ion Beam Irradiation

D. Oshima[1], T. Kato[2], S. Iwata[1]

[1]Institute of Materials and Systems for Sustainability, Nagoya University, Nagoya, Japan
[2]Department of Electronics, Graduate School of Engineering, Nagoya University, Nagoya, Japan

The magnetization process and switching field distribution (SFD) of ion beam patterned MnGa films were discussed based on the first order reversal curve (FORC) analysis and magnetic force microscope (MFM) observations. The FORC diagrams with so-called "boomerang" shape resulting from the increase of the interaction between "hysterons" that can be associated with ferromagnetic particles and/or domains were confirmed in the patterned MnGa with dot size larger than 520 nm. On the other hand, the shape of the FORC diagram became a simple Gaussian distribution, which is typical in the media comprised of well-isolated magnetic particles, for dot size smaller than 240 nm. The variation of the shape of FORC diagram was closely linked with the domain structure observed by MFM; multi-domain in the dot was confirmed for dot size larger than 520 nm while single domain for dot size less than 240 nm. The average switching field of the patterned film increased with decreasing the dot size, indicating that the dot edge damage and exchange interaction through ion irradiated regions were negligible in the ion beam patterned MnGa. The SFD also increased with decreasing the dot size. The SFD is considered to result from the existence of the pinning centers in the as-prepared MnGa and also from the dot size fluctuation of the resist masks fabricated by electron beam lithography. The optimization of the fabrication process will be effective to reduce SFD and sufficiently low SFD in high density MnGa BPM will be achieved by these process optimizations.

***Index Terms*—Bit patterned media, Ion beam irradiation, Switching field distribution, First order reversal curves, MnGa**

I. Introduction

BIT PATTERNED MEDIA (BPM) have attracted considerable interest as future high-density magnetic recording media because they provide a promising approach to solving the problem of the superparamagnetic limit, i.e., the thermal instability of recorded bits [1]. BPM are considered to extend the areal density of magnetic recording to more than 2 Tb/in^2, and also are expected to increase the areal density more than 5 Tb/in^2 by combining with other recording techniques such as heat and microwave assisted magnetic recordings. However, there are several issues to be solved for the practical use of BPM. One of the major issues is the development of a low-cost and high-yield fabrication process. The local ion irradiation technique is an attractive candidate since it makes the BPM fabrication flow simple compared to the conventional ion etching process. By using primary ions with appropriate mass and energy, the ion irradiation does not alter the surface morphology of the media and if it changes the magnetic properties of the media, the local ion irradiation results in magnetically patterned but topologically flat bit patterned structure, so-called planar BPM. Conventional ion etching process requires the flattening process, i.e., trench filling and polishing processes, to make the medium surface sufficiently flat for the stable flying of the recording head, and thus the flattening process makes the medium cost high and the fabrication yield low. Ion irradiation into Co/Pt [2]-[5] and Co/Pd [6], [7] multilayers was firstly studied to realize a planar BPM. However, in such materials, ion irradiation changes their easy axis from perpendicular to in-plane, and thus if planar BPM are fabricated using these materials, the perpendicular magnetized adjacent bits magnetically couple through the in-plane magnetized (ion-irradiated) region. This will limit the ultimate density of the BPM. In order to realize high density planar BPM, the materials whose magnetism is modified from ferromagnetic to paramagnetic by ion irradiation are desired. The ion dose dependence of magnetism of CoCrPt [8] and FePt [9], however, was reported to require high ion dose of ~ 10^{15} – 10^{16} ions/cm^2 to suppress their ferromagnetism.

Previously, we have reported that 30 keV Kr^+ ion irradiation altered the magnetism of $CrPt_3$ MnAl, and MnGa from ferromagnetic to nonmagnetic according to their phase change from the ordered to disordered phase [10]–[14]. In these materials, quite low dose ~ 10^{14} ions/cm^2 of the irradiation is sufficient to change them into nonmagnetic. We also demonstrated HDD-head-flyable planar BPM by taking the read-back signal from the ion irradiation patterned $CrPt_3$ medium [12]. These results indicate the ion irradiation technique is quite useful to fabricate high-density BPM. However, for the practical application, detailed study on the magnetic properties of the planar BPM, such as dot size dependence of the switching field and its distribution, is necessary. In this paper, we discuss in detail about the magnetization process and SFD of ion beam patterned MnGa films by analyzing the first order reversal curve diagrams.

II. Experimental Methods

The sample Cr (2 nm) / MnGa (15 nm) / Cr (20 nm) / MgO (001) substrate was prepared by RF magnetron sputtering deposition with a base pressure of ~ 1×10^{-7} Pa. The Cr buffer layer was grown on the MgO substrate at 400˚C and subsequently annealed at 600˚C for 60 min. The MnGa was grown on the Cr buffer layer by the co-sputtering of $Mn_{40}Ga_{60}$ and $Mn_{60}Ga_{40}$ targets at 300˚C, and subsequently annealed at 400 ˚C for 60 min. The top Cr layer was deposited as a protective layer after cooling to room temperature.

ZEP520A was used as a resist and dot patterned resist

masks were formed on the as-prepared film by electron beam lithography. The Kr^+ ion irradiation onto the sample was carried out by an ion implantation system. The ion energy and the beam current were set at 30 keV and 0.15 μA/cm^2, respectively. The ion dose was set at 1×10^{14} ions/cm^2 which was required for vanishing the ferromagnetism of the MnGa film completely. For measuring magnetic properties of ion beam patterned MnGa films, the patterned structure was fabricated in the area of 3×3 mm^2.

Magnetic properties were measured by an alternating gradient field magnetometer (AGM) at room temperature. The FORC measurements were also done by AGM. We used VARIFORC [17] to convert from measured FORCs to FORC diagrams.

X-ray diffraction (XRD) was utilized to analyze crystal structure. An atomic force microscope (AFM) and magnetic force microscope (MFM) were used to measure surface and magnetic structures, respectively. A scanning electron microscope (SEM) was also used for observation of resist masks.

III. Results and Discussions

Figure 1 shows (a) out-of-plane *M-H* loops and (b) XRD profiles of the MnGa film before and after ion irradiation with a dose of 1×10^{14} ions/cm^2. The as-prepared MnGa film showed a square hysteresis loop with a large perpendicular anisotropy, the value of which was estimated to be $\sim 7 \times 10^6$ erg/cc from the in-plane curve (not shown here). As shown in Fig. 1 (b), MnGa 001 and 002 peaks were clearly observed in the as-prepared film, which indicates the formation of $L1_0$-ordered MnGa phase. Besides these peaks, only diffraction peaks from MgO(001) substrate and Cr buffer layer were seen, indicating MnGa films have (001) orientation. The ordering parameter estimated from integrated intensities of superlattice 001 and fundamental 002 peaks was almost unity, which means the as-prepared MnGa have fully ordered $L1_0$ structure with (001) orientation. The ferromagnetism and large perpendicular anisotropy of the film originate from the (001) oriented $L1_0$-ordered phase. After the ion irradiation, the ferromagnetism of the MnGa film disappeared as shown in Fig. 1 (a) and the MnGa 001 peak disappeared and 002 peak shifts toward lower-angle side as seen in Fig. 1 (b). This is due to the phase change of the MnGa from $L1_0$-ordered phase to A1-disordered one.

Figure 2 shows ion dose dependences of saturation magnetization M_s, coercivity H_c, and perpendicular anisotropy K_u of MnGa films irradiated with 30 keV Kr^+ ions. These values were normalized as the values before the irradiation to be 1. The M_s and K_u of the MnGa gradually decreased with increasing the ion dose. The H_c of MnGa slightly increased with increasing the ion dose up to $\sim 10^{13}$ ions/cm^2, and then decreased with further increase of the ion dose. One will note that the K_u of the MnGa decreased in proportion to M_s. This implies that the increase of the ion dose results in the increase of the volume of nonmagnetic A1- phase MnGa created by the ion irradiation as shown in the schematic illustrations of Fig. 3.

Figure 3 shows schematics of expected microstructure of the MnGa film uniformly irradiated with Kr^+ ions. The surface atomic density of (001) plane of the MnGa is 1.3×10^{15} cm^{-2}, and thus the ion dose of 10^{13} ions/cm^2 corresponds to one ion per 3 nm × 3 nm square. It is considered that such ion dose creates local nonmagnetic A1-MnGa cylinders, and the ferromagnetic $L1_0$-MnGa nano-crystals will be surrounded by the nonmagnetic A1-MnGa matrix as shown in Fig. 3. The increase of H_c with increasing the ion dose up to $\sim 10^{13}$ ions/cm^2 shown in Fig. 2 is also understood by this model; ion dose creates the nonmagnetic pinning center of the domain wall which will impede of the smooth propagation of the domain wall. Further increase of the ion dose will reduce the volume of the $L1_0$-MnGa nano-crystals which will results in the decrease of H_c due to the reduction of the product of K_uV, where V is the volume of $L1_0$-MnGa nano-crystal. The model of the microstructure of the ion irradiated MnGa shown in Fig. 3 also supported by the experimental results of variations of X-ray magnetic circular dichroism (XMCD) and low-temperature magnetic hysteresis loops of the ion irradiated MnGa [16]. The XMCD spectra shapes did not change with the ion dose, which means the ferromagnetic regions have the same electronic structure to that of as-prepared MnGa [16]. The coercivity of the ion irradiated MnGa significantly increased with lowering temperature, supporting the existence of the ferromagnetic nano-crystals surrounded by the nonmagnetic A1-MnGa matrix as shown in Fig. 3. From the

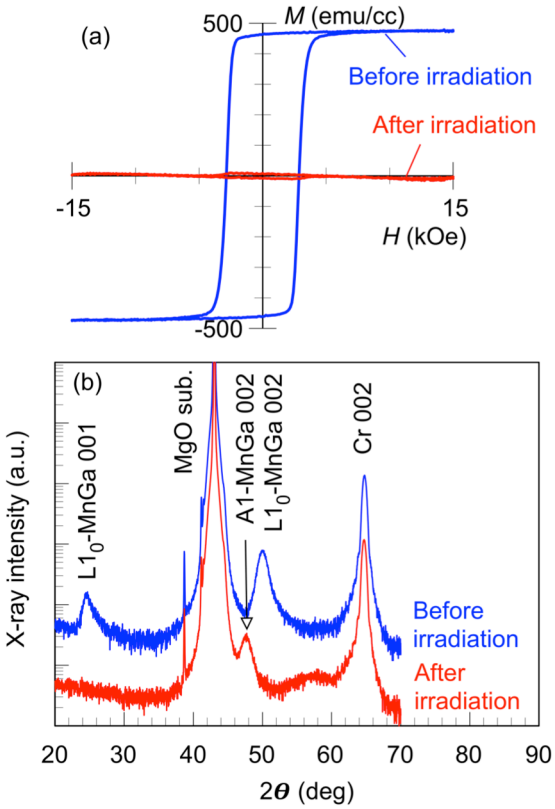

Fig. 1 (a) out-of-plane *M-H* loops and (b) XRD profiles of the MnGa film before and after the ion irradiation with a dose of 1×10^{14} ions/cm^2 of 30 keV Kr^+ ions.

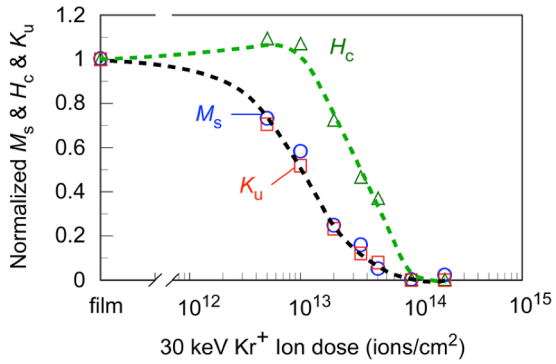

Fig. 2 Ion dose dependences of saturation magnetization M_s, coercivity H_c, and perpendicular anisotropy K_u of MnGa films with irradiated with 30 keV Kr^+ ions. These values are normalized as the values before the irradiation to be 1.

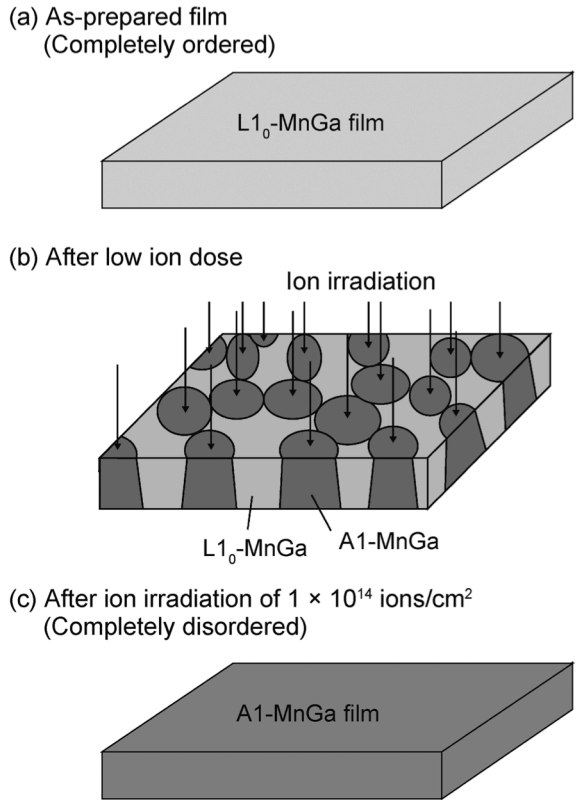

Fig. 3 Schematic illustrations of the variation of the microstructure of MnGa films with increasing the ion dose. (a) as-prepared, (b) low dose of ion irradiation, (c) ion dose more than 1 × 10^{14} ions/cm^2.

model of the microstructure shown in Fig. 3, we believe the ion irradiated MnGa comprises of two phases: $L1_0$-ordered and A1-disordered phases and has no intermediate phase with low K_u and low H_c. This will be beneficial to reduce SFD in high-density planar BPM, since the SFD is considered to be significantly increased by the existence of the low K_u and low H_c regions at bit boundaries, which is expected in conventional BPM fabricated by ion etching process.

Figure 4 shows MFM images of as-prepared and ion-beam patterned MnGa films with various dot sizes. These images were taken after demagnetizing the samples by alternating magnetic fields. Bright and dark contrasts indicate the magnetization up and down in the film normal direction, respectively, and intermediate contrast is coming from the nonmagnetic MnGa created by the local ion irradiation. As seen in Fig. 4 (a), maze domains are formed on the as-prepared film reflecting the large perpendicular anisotropy in the (001) oriented $L1_0$-MnGa film. Figs. 4 (b) – (g) show MFM images of ion beam patterned MnGa films. For the images of ion beam patterned MnGa films, clear bright and dark magnetic contrasts were observed in "bit" regions while no magnetic contrast was seen in "space" regions surrounding the bit regions because the space regions were exposed to the ion beam irradiation and have no magnetization due to the phase change from $L1_0$ to A1 phase as discussed in Figs. 1 – 3. Multidomain structures are observed in bit regions of the ion beam patterned MnGa with the pitch size down to 500 nm.

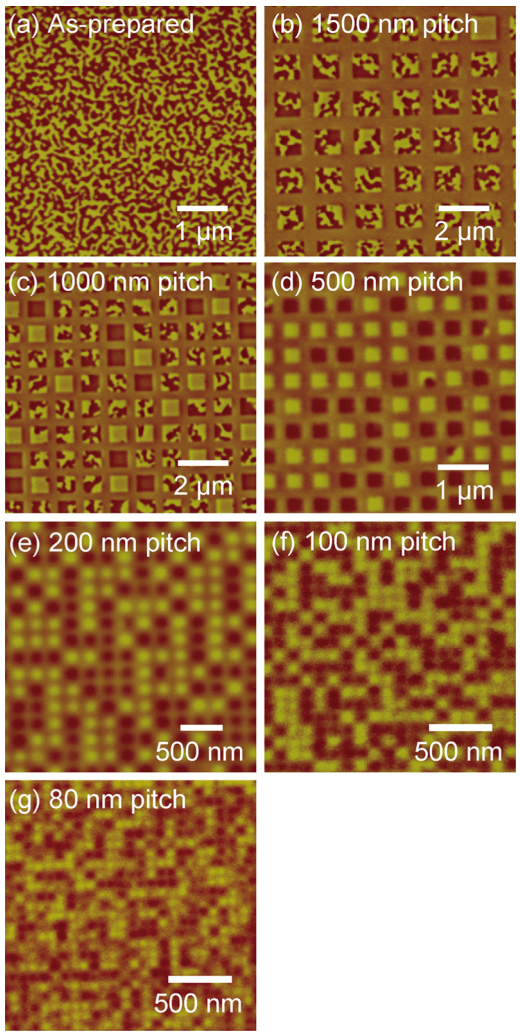

Fig. 4 MFM images of (a) as-prepared and ion-beam patterned MnGa film with pitch sizes of (b) 1500, (c) 1000, (c) 500, (e) 200, (f) 100, and (g) 80 nm. These images were taken after AC demagnetizing.

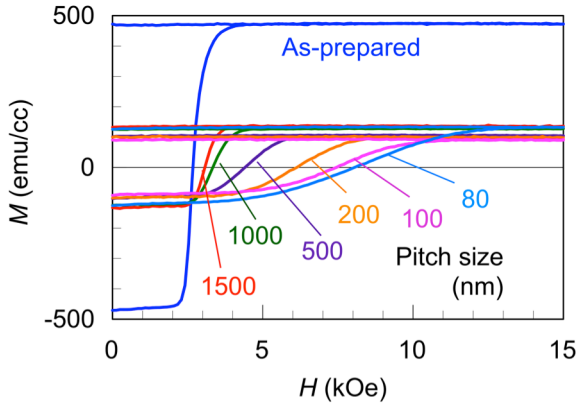

Fig. 5 *M-H* loops of as-prepared and bit patterned MnGa films with pitch sizes of 1500, 1000, 500, 200, 100 and 80 nm. The values of the saturation magnetizations were normalized by the volumes of the MnGa films irrespective of the pitch size.

TABLE 1
Sizes of pitch, dot, and spacings of the fabricated patterned films

Pitch size (nm)	Dot size (nm)	Spacing (nm)
1500	810	690
1000	520	480
500	240	260
200	90	110
100	50	50
80	44	36

Further decrease of pitch size changes the domain structure from multidomain to single domain. It is anticipated that magnetization reversal process changes across the pitch size of ~ 200 nm associated with the change of the domain structure. The nonmagnetic spaces are effective to suppress exchange coupling between ferromagnetic bits through the spaces, which is the major problem to fabricate high-density planar BPM using Co/Pt [2]–[5] and Co/Pd [6], [7]. By using MnGa, however, the planar BPM with a pitch size down to 80 nm were found to be fabricated. Further reduction of the pitch size is expected by fabricating fine resist masks with pitch size less than 80 nm.

Figure 5 shows *M-H* loops of the as-prepared and ion-beam patterned MnGa films with various designed pitch sizes. The values of the saturation magnetizations were normalized by the volume of the MnGa films irrespective of the pitch size of the patterned MnGa. The saturation magnetization M_s decreased after the patterning since the space regions become nonmagnetic by the ion irradiation with the dose of 1×10^{14} ions/cm^2. Dot sizes of the patterned MnGa films were estimated by comparing the saturation magnetization of the patterned MnGa with that of as-prepared MnGa. From the designed pitch size and estimated dot size, the dot spacing was easily evaluated, which is summarized in Table 1. The estimated dot sizes agreed well with those estimated from MFM images shown in Fig. 3. The coercivity H_c of the patterned samples increased with decreasing the pitch (dot) size. The increase in coercivity is considered to be due to the change of the magnetization process from domain wall motion to coherent rotation.

In order to discuss the magnetization process of the ion beam patterned MnGa, FORCs were measured and analyzed. For FORC measurements, a positive saturation field H_{sat} was initially applied to the sample. After the saturation, the field was decreased from H_{sat} to a reversal field H_r, and then magnetization $M(H, H_r)$ was measured with increasing the external field H back to H_{sat}. A set of FORCs was obtained with various reversal fields as shown in Fig. 6. A FORC diagram is a contour plot of $\rho(H, H_r)$ defined as

$$\rho(H,H_r) = -\frac{1}{2}\frac{\partial M(H,H_r)}{\partial H \partial H_r}. \quad (1)$$

The axes are rotated by changing coordinates from $\{H, H_r\}$ to $\{H_c, H_b\}$ where $H_c = (H - H_r) / 2$ and $H_b = (H + H_r) / 2$. The H_c and H_b correspond to the local coercivity and local bias field, respectively. Preisach model [18] generalize a hysteresis loop as a sum of rectangular hysteresis loops called "hysterons" which has a single domain state with magnetization of $+m$ or $-m$ and has two parameters of coercivity and bias field. Pike *et. al*. showed that the FORC diagram provides information about distributions of local coercivity $f(H_c)$ and bias field $g(H_b)$ [19] of constituent magnetic particles as

$$\rho(H_c,H_b) = f(H_c)g(H_b). \quad (2)$$

Figure 7 shows FORC diagrams of the ion-beam patterned MnGa films with various dot sizes. The shape of the diagrams changes with decreasing the dot size as shown in the figures. For FORC diagrams taken from the patterned MnGa films with dot size less than 240 nm, the FORC distributions were found to have a simple distribution expressed as eq. (2). Therefore, the hysteresis loops of the patterned films with small dot sizes are represented by the sum of magnetically isolated hysterons (single domain particles) as in the Preisach model. This indicates that the exchange interaction between dots through an ion irradiated region is negligibly weak in the

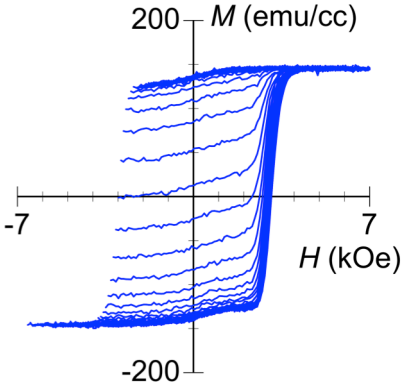

Fig. 6 FORCs of the ion beam patterned MnGa film with a pitch size of 1500 nm.

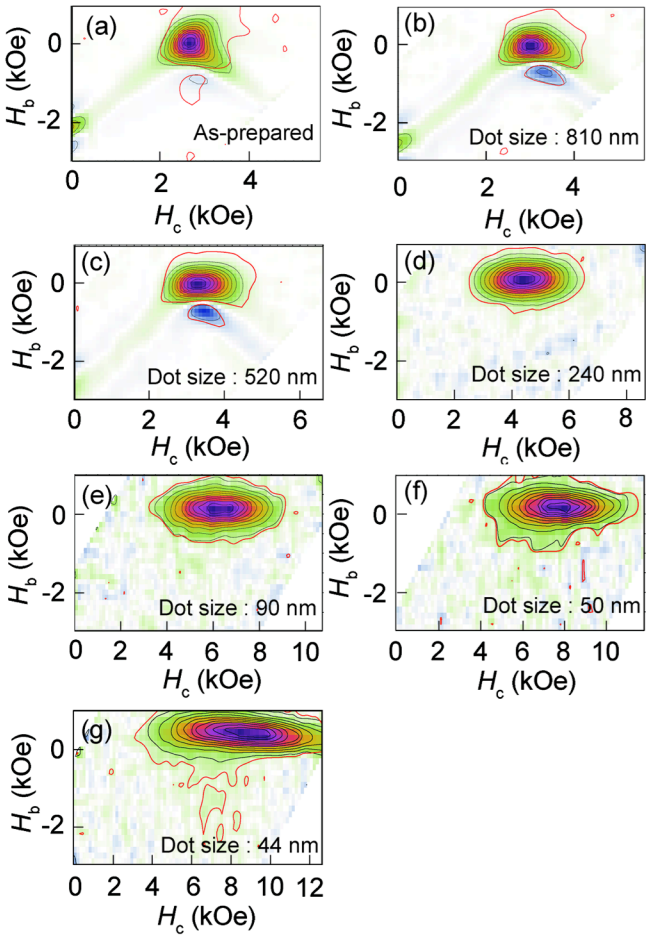

Fig. 7 FORC diagrams of (a) as-prepared and ion-beam patterned MnGa film with dot sizes of (b) 810, (c) 520, (d) 240, (e) 90, (f) 50 and (g) 44 nm. The dot sizes were estimated from the saturation magnetization of the patterned MnGa shown in Fig. 5.

ion irradiated patterned MnGa film. The distribution of the interaction field is considered to be mainly due to the dipole interaction between the dots, which will also contribute to widen the coercivity distribution, SFD, which should be as small as possible for the practical application of BPM. In terms of the dipole interaction, the MnGa film is preferable since it has a relatively low M_s of ~ 500 emu/cc compared to an $L1_0$-FePt film. The FORC diagrams of the as-prepared and patterned film with dot sizes larger than 500 nm have so-called "boomerang" shapes, extending the $\rho(H_c, H_b)$ in diagonal directions as shown in the figures. Furthermore, a negative $\rho(H_c, H_b)$ region exists underneath the positive main peak of the $\rho(H_c, H_b)$ around $H_b \approx 0$ line. These features have been observed in other systems [20, 21] and also observed in FORC diagrams calculated based on the moving Preisach model in which magnetization process of hysterons depends both on the external field and the average magnetization state of the film [19]. It may be reasonable to consider the moving Preisach model since the as-prepared and patterned MnGa with large dot sizes have multidomain structures as shown in

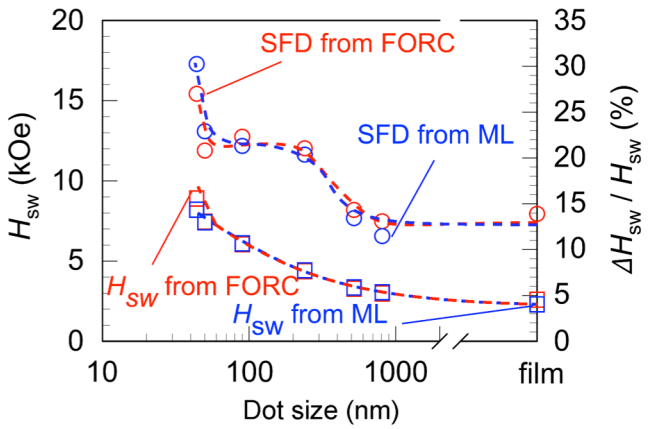

Fig. 8 Dot size dependences of H_{sw} and $\Delta H_{sw}/H_{sw}$ estimated both from FORCs and MLs of the ion-beam patterned MnGa films.

the MFM images in Fig. 4, and their magnetization processes are dominated by the nucleation and domain wall propagation, which may be expressed by strongly coupled hysterons with each other. From these results, the magnetization reversal process of the ion-beam patterned MnGa film changed at the dot size around 240 nm. We compared this value with the critical size that the MnGa dot becomes a single domain state. The critical size was calculated from saturation magnetization M_s of 450 emu/cc, perpendicular anisotropy of K_u of 7×10^6 erg/cc, and exchange stiffness which was assumed to be 0.5×10^{-6} erg/cm. By comparing the energy of two cases between single domain state and two domain state with one domain wall inside a dot, the critical size to realize the single domain was simply estimated to be ~ 80 nm. This is much smaller than the value (~240 nm) at which the magnetization reversal process changed as discussed from FORC diagram shown in Fig. 7.

By fitting Gaussian profiles to the line profile of H_c at H_b = 0 in the FORC diagrams, the average switching field H_{sw} and standard deviation ΔH_{sw} were estimated. Figure 8 shows dot size dependences of the H_{sw} and the SFD defined as $\Delta H_{sw}/H_{sw}$. The H_{sw} and SFD estimated by fitting error functions to the major loops (MLs) of bit patterned MnGa in Fig. 5 are also shown in Fig. 8. The H_{sw} of the as-prepared MnGa film was estimated from the coercivity of its ML since the ML of the as-prepared film was not expressed by the simple error function. The H_{sw} and SFD estimated from both MLs and FORCs agreed well with each other except for the samples with dot sizes below 50 nm. Based on the Preisach model, the FORC diagram will separate the contributions of coercivity distribution of dots and interaction field such as the stray field from surrounding dots. For the sample with dot size of 50 nm and spacing of 50 nm, the stray field of ~300 Oe was estimated, which is roughly consistent with the difference in SFD between FORC and MLs as in Fig. 8. Thus, we think FORC analysis will give precise H_{sw} and SFD compared to the ML analysis especially in the samples with small dot sizes.

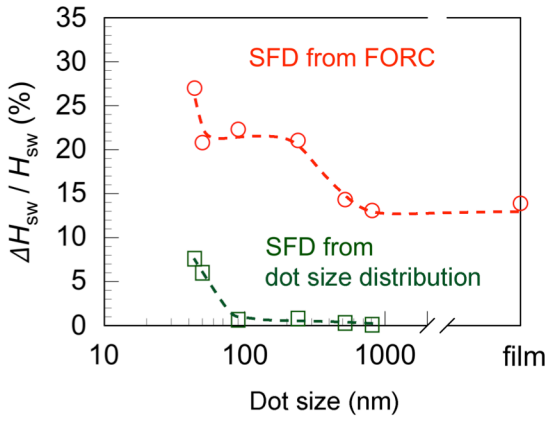

Fig. 10 Dot size dependence of SFD estimated from FORC analysis and calculated assuming the dot size distribution.

The average switching field H_{sw} of the ion beam patterned MnGa increased with decreasing the dot size. Shaw *et al*. reported the reduction of the switching field with decreasing the dot size for ion milled Co/Pd nanostructures [22], which is due to the dot edge damage, i.e., the existence of low K_u regions at the dot edge. In our samples, H_{sw} increased with decreasing the dot size, which is similar to the trend of the pre-patterned Co/Pd nanostructures in Ref. [22]. Thus we believe that the dot edge damage of the ion beam patterned MnGa is negligibly small and the exchange coupling between the dots through ion irradiated regions is also negligible. For samples with dot size larger than 520 nm, the SFD seems to be almost constant ~ 13 %. In these samples, the magnetization reversal process is considered to be dominated by nucleation and domain wall propagation. Therefore, the SFD in these samples is considered to depend on the areal density of the pinning centers existing in the as-prepared MnGa film, which means that the SFD will be decreased by improving the quality of the MnGa films. The SFD increased from 13 to 20 % when the dot size became less than 240 nm. This increase is considered to be related to the transition of the magnetization reversal process as discussed in Figs. 4 and 7. For samples with dot size smaller than 240 nm, the switching is not dominated by nucleation and domain wall propagation, which means that switching field is rather dominated by local distribution of magnetic properties such as perpendicular anisotropy and saturation magnetization which result from fluctuations of crystal orientation and degree of order. We consider that improving the quality of the MnGa films will also decrease large SFD below the dot size of 240 nm.

Further increase of the SFD was observed when the dot size is less than 50 nm as shown in Fig. 8. We considered dot size distribution as one of the origins for the increase of SFD in the small dot size MnGa. To estimate the dot size distribution of the ion beam patterned MnGa, we measured size distribution of the resist mask by SEM observation, since it is difficult to estimate the dot size distribution in an ion-beam patterned film. In the ion beam patterned MnGa, the dot size may be roughly estimated by using MFM observation, but the dot size estimated from MFM observation contains errors due to the size of the magnetic tip for MFM observation.

Figure 9 shows SEM images of dot patterned resist masks after the ion irradiation process (before stripping the resist masks). The average dot size estimated from the SEM observations agrees well with that estimated from the decrease of the M_s of the ion-beam patterned films discussed in Fig. 5. This implies that the lateral distribution of the incident ions in MnGa will be limited within a few nanometers, and the magnetic pattern of the ion irradiated MnGa is almost identical to the resist pattern. This is also supported by transmission electron microscope observations of the bit boundary of ion beam patterned $CrPt_3$, in which the lateral struggling of ~ 5 nm was expected under the condition of the Kr^+ ion irradiation into $CrPt_3$ with an energy of 30 keV [15].

The dot size distribution (more exactly, resist size distribution) ΔD was estimated to be around 3 nm for all the patterns. By using the ΔD and the dependence of the H_{sw} on the average dot size, we can simply calculate the SFD as $(\partial H_{sw} / \partial D)\ \Delta D / H_{sw}$., where $\partial H_{sw} / \partial D$ was estimated from Fig. 8. Figure 10 shows the SFDs calculated considering the dot size distribution. The SFD estimated from FORC analysis are also shown in the figure. The calculated SFDs due to the dot size distributions abruptly increased below the dot size of 100 nm. This tendency is also seen in the SFDs estimated from the FORC analysis, and thus one of the reasons for the increase of the SFD in the samples with dot size below 50 nm may be the dot size distributions of the resist mask. The reduction of the dot size distribution is considered to make the SFD low in BPM with small dot sizes. The dot size distribution will be controlled by optimizing the EB fabrication process, e.g., the

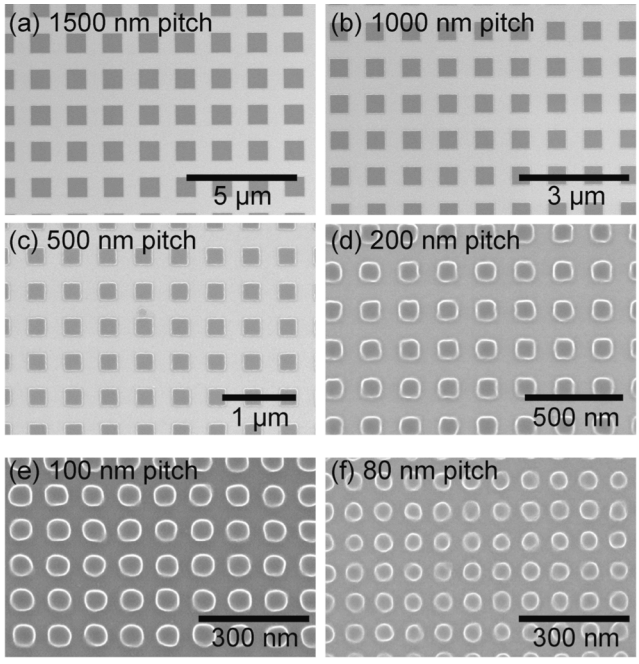

Fig. 9 SEM images of dot patterned resist masks with pitch sizes of (a) 1500, (b) 1000, (c) 500, (d) 200, (e) 100, and (f) 80 nm. These images were taken after the ion irradiation process.

reduction of the resist thickness will be effective to reduce the dot size distribution. In this case, however, the energy of primary ions for magnetic patterning is required to be reduced since the resist should be thick enough to stop irradiated ions for the fabrication of planar BPM. In addition to the optimization of the patterning processes, the quality of the as-prepared film should be improved since the SFD of 10–15 % is considered to result from the existence of the pinning centers in the as-prepared MnGa film. Thus high-density ion beam patterned planar BPM are expected by improving the film quality and optimizing the fabrication process which will result in sufficiently low SFD for the practical application of planar BPM.

IV. Conclusion

The magnetism of the MnGa film was transferred from ferromagnetic to non-magnetic (paramagnetic) by 30 keV Kr^+ ion irradiation with a dose of 1×10^{14} ions/cm^2 due to the phase change from $L1_0$ ordered to A1 disordered phase. The transition of the magnetism is considered to proceed through the increase of the volume of the A1 disordered phase created by ion irradiation, and the MnGa irradiated below 1×10^{14} ions/cm^2 is considered to have the microstructure that ferromagnetic $L1_0$ ordered MnGa nanocrystals exist in nonmagnetic A1 disordered MnGa matrix. Thus the bit boundary of the ion beam patterned MnGa, in which the ion irradiation below 1×10^{14} ions/cm^2 is expected to be sharp, which will result in the small SFD even in the high density BPM.

The ion beam patterned MnGa films were fabricated by using EB lithography and the ion irradiation with a dose of 1×10^{14} ions/cm^2. The magnetization process and the SFD of the patterned MnGa films were analyzed by FORC analysis. The so-called "boomerang" shape of the FORC diagram was confirmed in the patterned films with dot sizes larger than 520 nm, while the simple Gaussian distribution of the FORC diagram was observed in the samples with dot size smaller than 240 nm. The variation of the FORC diagrams is related to the magnetization process; nucleation and domain wall propagation dominates the switching process for dot size larger than 520 nm and magnetization switching of well-isolated magnetic particles is considered for bit size smaller than 240 nm. The average switching field of the patterned film increased with decreasing dot size, indicating that the dot edge damage and exchange interaction between the dots are negligibly small in the ion beam patterned MnGa. The SFD also increased with decreasing dot size. The SFD of the as-prepared MnGa was around 13%, and it increased to 20% when the dot size becomes less than 240 nm. This increase may be due to the change of the switching process. Further increase of the SFD was confirmed with decreasing the dot size less than 50 nm, and this increase of the SFD may come from dot size fluctuations. From these results, improvement of the film quality of the as-prepared MnGa and optimization of the fabrication process of the resist mask will be effective to reduce SFD, and sufficiently low SFD in high density MnGa BPM will be achieved by these process optimizations.

In this study, we reported ion beam patterned MnGa with the dot size down to 44 nm, which is not sufficient to realize high density BPM. In our previous report [15], the transition width between "bit" and "spacing" in a ion beam patterned $CrPt_3$ film was estimated to be ~ 5 nm under the condition of 30 keV Kr^+ irradiation, which was consistent with the lateral struggling of incident ions estimated from transport ion in matter (TRIM) simulations. The simulation predicts the transition width can be reduced down to ~ 1 nm by using 5 keV Xe^+ ions [15]. Thus we expect the dot size around 6 nm and dot spacing around 2 nm, which corresponds to the areal density of 10 Tb/in^2. The thermal stability of the MnGa is also crucial to achieve high density BPM using MnGa. The dot size MnGa with a thickness of 10 nm can be reduced to 5.6 nm under the constraint of the thermal stability factor of 60. Thus, we consider ion irradiation onto MnGa is quite attractive to achieve ultra high density planar BPM.

Acknowledgment

The authors thank Mr. M. Kumazawa of Nagoya University for his assistance with the experiments. The authors are grateful for financial support by Grants-in-Aids for Scientific Research from the Ministry of Education, Culture, Sports, Science and Technology.

References

[1] A. Kikitsu, Y. Kamata, M. Sakurai, and K. Naito, "Recent Progress of Patterned Media," *IEEE. Tran. Magn*., vol. 43 (2007), pp. 3685-3688.

[2] C. Chappert, H. Bernas, J. Ferré, V. Kottler, J.-P. Jamet, Y. Chen, E. Cambril, T. Devolder, F. Rousseaux, V. Mathet, and H. Launois, "Planar Pattened Magnetic media Obtained by Ion Irradiation," *Science*, vol. 280 (1998), pp. 1919-1922.

[3] B. D. Terris, L. Folks, D. Weller, J. E. E. Baglin, J. Kellock, H. Rothuizen, and P. Vettiger, "Ion-beam patterning of magnetic films using stencil masks," *Appl. Phys. Lett.,* vol. 75 (1999), pp. 403-405.

[4] J. Ferré, C. Chappert, H. Bernas, J.-P. Jamet, P. Meyer, O. Kaitasov, S. Lemerle, V. Mathet, F. Rousseaux, and H. Launois, "Irradiation induced effects on magnetic properties of Pt/Co/Pt ultrathin films," *J. Magn. Magn. Mater.*, vol. 198–199 (1999), pp. 191-193.

[5] R. Hyndman, P. Warin, J. Gierak, J. Ferré, J. N. Chapman, J. -P. Jamet, V. Mathet, and C. Chappert, "Modification of Co/Pt multilayers by gallium irradiation – Part 1 : The effect on structural and magnetic properties," *J. Appl. Phys*., vol. 90 (2001), pp. 3843-3849.

[6] E. Suharyadi, S. Natsume, T. Kato, S. Tsunashima, and S. Iwata, "Microstructure and magnetic properties of the FIB irradiated Co/Pd multilayer films," *IEEE Trans. Magn*., vol. 41 (2005), pp. 3595-3597.

[7] E. Suharyadi, T. Kato, S. Tsunashima, and S. Iwata, "Magnetic Properties of Patterned Co/Pd Nanostructures by E-Beam Lithography and Ga Ion Irradiation," *IEEE Trans. Magn.,* vol. 42 (2006), pp. 2972-2974.

[8] T. Hinoue, K. Ito, Y. Hirayama, and Y. Hosoe, "Effects of lateral straggling of ions on patterned media fabricated by nitrogen ion implantation," *J. Appl. Phys*., vol. 111 (2012), 07B912.

[9] N. Gaur, S. Kundu, S. N. Piramanayagam, S. L. Maurer, H. K. Tan, S. K. Wong, S. E. Steen, H. Yang, and C. S. Bhatia, "Lateral displacement induced disorder in $L1_0$-FePt nanostructures by ion-implantation," *Sci. Rep*., vol. 3 (2013), 1907.

[10] T. Kato, S, Iwata, Y. Yamauchi, and S. Tsunashima, "Modification of magnetic properties and structure of Kr^+ ion-irradiated $CrPt_3$ films for planar bit patterned media," *J. Appl. Phys*., vol. 106 (2009) 053908.

[11] D. Oshima, M. Tanimoto, T. Kato, Y. Fujiwara, T. Nakamura, Y. Kotani, S. Tsunashima, and S. Iwata, "Modifications of Structure and Magnetic

Properties of $L1_0$ MnAl and MnGa Films by Kr^+ Ion Irradiation," *IEEE Trans. Magn.,* vol. 50 (2014) 3203407.

[12] T. Kato, S. Iwata, Y. Yamauchi, S. Tsunashima, K. Matsumoto, T. Morikawa, and K. Ozaki, "Planar patterned media fabricated by ion irradiation into $CrPt_3$ ordered alloy films," *J. Appl. Phys*., vol. 105 (2009) 07C117.

[13] D. Oshima, T. Kato, S. Iwata, and S. Tsunashima, "Control of Magnetic Properties of MnGa films by Kr^+ Ion Irradiation for Application to Bit Patterned Media," *IEEE Trans. Magn*., vol.49 (2013), pp. 3608-3611.

[14] E. Suharyadi, D. Oshima, T. Kato, and S. Iwata, "Switching field distribution of planar-patterned $CrPt_3$ nanodots fabricated by ion irradiation," *J. Appl. Phys*., vol. 109 (2011), 07B771.

[15] D. Oshima, E. Suharyadi, T. Kato, and S. Iwata, "Observation of ferri-nonmagnetic boundary in $CrPt_3$ line–and-space patterned media using a dark-field transmission electron microscope," *J. Magn. Magn. Mater*., vol. 324 (2012) pp. 1617-1621

[16] D. Oshima, M. Tanimoto, T. Kato, Y. Fujiwara, T. Nakamura, Y. Kotani, S. Tsunashima, and S. Iwata, "Ion Irradiation-Induced Magnetic Transition of MnGa Alloy Films Studied by X-Ray Magnetic Circular Dichroism and Low-Temperature Hysteresis Loops," *IEEE Trans. Magn.,* vol. 52 (2016), 3201804.

[17] R. Egli, "VARIFORC: An optimized protocol for calculating non-regular first-order reversal curve (FORC) diagrams, *Glob. Planet. Change*, vol. 110 (2013), pp.302-320.

[18] I. D. Mayergoyz and G. Friedman, "GENERALIZED PREISACH MODEL OF HYSTERESIS," *IEEE Trans. Magn.*, vol. 24, pp.212-217.

[19] C. R. Pike, A. P. Roberts, and K. L. Verosub, "Characterizing interactions in fine magnetic particle systems using first order reversal curves," *J. Appl. Phys.*, vol. 85 (1999), pp.6660-6667.

[20] D. A. Gilbert, G. T. Zimanyi, R. K. Dumas, M. Winklhofer, A. Gomez, N. Eibagi, J. L. Vicent and K. Liu, "Quantitative Decoding of Interactions in Tunable Nanomagnet Arrays Using First Order Reversal Curves," *Sci. Rep.*, vol. 4 (2014), 4204.

[21] D. A. Gilbert, J.-W. Liao, L.-W. Wang, J. W. Lau, T. J. Klemmer, J.-U. Thiele, C.-H. Lai, and K. Liu, "Probing the $A1$ to $L1_0$ transformation in FeCuPt using the first order reversal curve method," *APL Mater*., vol. 2 (2014), 086106.

[22] J. M. Shaw and S. E. Russek, "Reversal mechanisms in perpendicularly magnetized nanostructures," *Phys. Rev. B*, vol. 78 (2008), 024414.